Article

A Theoretical Design of Chiral Molecules through Conformational Lock towards Circularly Polarized Luminescence

Lewen Wang [1], Tengfei He [2], Hailiang Liao [1], Yige Luo [1], Wen Ou [1], Yinye Yu [1,3,4], Wan Yue [1], Guankui Long [2], Xingzhan Wei [3] and Yecheng Zhou [1,*]

[1] Guangzhou Key Laboratory of Flexible Electronic Materials and Wearable Devices, School of Materials Science and Engineering, Sun Yat-sen University, Guangzhou 510006, China; wanglw29@mail2.sysu.edu.cn (L.W.); liaohl3@mail2.sysu.edu.cn (H.L.); lyg1520@126.com (Y.L.); ouwen3@mail2.sysu.edu.cn (W.O.); yuyinye@cigit.ac.cn (Y.Y.); yuew5@mail.sysu.edu.cn (W.Y.)
[2] School of Materials Science and Engineering, National Institute for Advanced Materials, Renewable Energy Conversion and Storage Center (RECAST), Nankai University, Tianjin 300350, China; hetf2021@nankai.edu.cn (T.H.); longgk09@nankai.edu.cn (G.L.)
[3] Micro-Nano Manufacturing and System Integration Center, Chongqing Institute of Green and Intelligent Technology, Chinese Academy of Sciences, Chongqing 400714, China; weixingzhan@cigit.ac.cn
[4] University of Chinese Academy of Sciences, No. 19A Yuquan Road, Shijingshan District, Beijing 100049, China
*   Correspondence: zhouych29@mail.sysu.edu.cn

Abstract: Circularly polarized (CP) light has shown great potential in quantum computing, optical communications, and three-dimensional displays. It is still a challenge to produce high-efficiency and high-purity CP light. Herein, we proposed a strategy to design chiral organic small molecules for CP light generation. These kinds of chiral molecules are formed by achiral light-emitting groups and achiral alkyl chains through conformational lock, which indicates that chirality can also be introduced into achiral light-emitting groups through rational molecular design. The chirality of these molecules can be further tuned by changing the length of the alkyl chains connecting the diketopyrrolopyrrole unit. The chiroptical properties of these molecules are confirmed by calculated electronic circular dichroism and chiral emission spectra, and further confirmed in experiments. The strategy developed in this work will greatly enlarge the candidate library of chiral luminescent materials.

1. Introduction

Chirality is a fundamental geometric property of an object, from elementary particles to amino acid, protein, DNA, and human hands. Artificial chiral materials have been widely used in biopharmaceuticals and artificial proteolytic catalysis [1]. Recently, chiral materials have become a hot research topic [2–7] since they have promising applications in circularly polarized organic light-emitting diodes (CP-OLEDs) [8,9], chiral switches [10] and chiral sensors [11–13].

Circularly polarized (CP) light has tremendous potential applications in encrypted data transport [14], quantum computing [15], optical communication for spintronics [16,17], and three-dimensional displays [18]. Traditionally, CP light is produced by filtering a non-polarized light with structures or devices [19,20]. Cai et al. demonstrated a silicon-based compact optical CP laser emitter, which embedded multiple angular grating structures into the whispering gallery mode (WGM) resonance. The WGM resonance gives the incident laser a refined orbital angular momentum [21]. However, in these devices, the laser needs to go through several extra elements, which consume extra energy and then decrease the efficiency of luminescence. Besides, the laser device structure is difficult to simplify due to these extra optical elements. The other method is generating CP light directly from chiral

materials, which could remove the bulky optical elements and then decrease the production cost. Additionally, the removal of optical elements will diminish energy loss and improve power conversion efficiencies [22]. Due to structure variety, only limited inorganic materials can produce CP light [23]. Thus, chiral organic or organic-inorganic hybrid materials are developed. However, organic-inorganic hybrid materials must improve the stability [24,25].

Recently, using organic light-emitting diodes (OLEDs) to generate CP light has been emerged and successfully realized [2,4]. In order to fabricate the CP-OLEDs with a high *g*-factor (the dissymmetry factor of CP light, includes g_{abs} and g_{lum} which are the circularly polarized absorption dissymmetry factor and the photoluminescence dissymmetry factor, respectively) and high brightness, three strategies have been applied. The first strategy is generating CP light using polymers or oligomers that bear pendant chiral side chains on achiral conjugated polymer backbones [26,27], as shown in Figure 1a. By synthesizing and characterizing a series of co-polymer with chiral or achiral side chains, Kulkarni found that chiral side chains on fluorene units are the key to forming cholesteric liquid crystalline phase after annealing, which leads to strong chiroptical properties, with dissymmetry factor of electroluminescence (g_{EL}) reaching -0.62 [26].
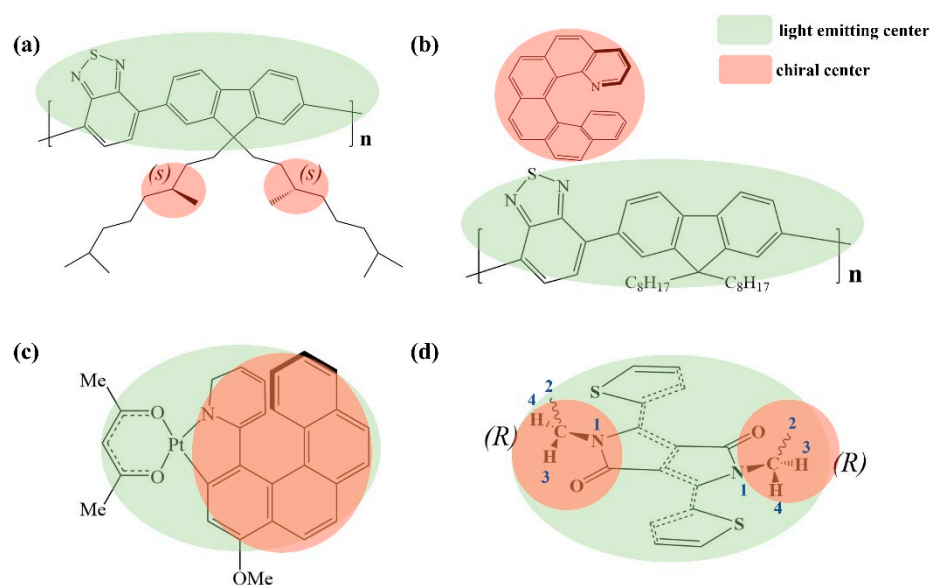
Figure 1. Typical CP light-emitting materials: (**a**) conjugated polymer with chiral side chains; (**b**) mixing an achiral light-emitting molecule with chiral molecules; (**c**) small molecule with light-emitting center overlaps with the chiral center; and (**d**) the proposed chiral materials by adding an achiral side chain to the achiral light-emitting core, then the chirality is introduced.

The second strategy is adding chiral additives into a conventional achiral luminescent polymer to achieve CP light. As illustrated in Figure 1b, Yang et al. blended helicene enantiomer into the conventional polymer LED, and successfully fabricated high-performance CP-OLED. The helicene dopant introduces chirality into the achiral polymer without a dramatic decrease in the LED performance, and the g_{EL} factor of this CP-OLED can be increased to 1.0 [28]. The chiral additive induces the non-polarized light emission into right-handed or left-handed light emission [29]. However, there is a trade-off between the *g* factor and the device efficiency in the first and second strategies. A high *g* factor usually results in low performance.

The third strategy is generating CP light directly from small chiral organic molecules. For example, Brant et al. fabricated a circular polarized phosphorescent OLED (CP-PHOLED) by using a chiral platinahelicene complex, which possessed a sufficiently high g_{EL} value of up to 0.79 together with higher luminance (19% higher than that of the conventional OLEDs with antiglare filter). Therefore, such chiral organic molecule can dramatically

decrease the power consumption and allow devices to operate at a lower voltage [8,30]. This work raises the promising future of small chiral organic dyes for application in CP laser.

As shown in Figure 1a,b, the chiral part (side chain) and the light-emitting part (polymer backbone) are separated in the first and second strategy, which leads to lower performance or low g_{EL} factor. In the third strategy, as shown in Figure 1c, small molecules integrate both the light-emitting center and the chiral center in the same functional group, overcoming the issue between efficiency and g_{EL} factor [31]. However, the number of chiral light-emitting conjugation materials is still limited.

Inspired by pioneer research [32–34], here we put forward a new strategy to design chiral light-emitting molecules that the chiral center is formed by both the achiral light-emitting backbone and the achiral side chain. This strategy suggests that most traditionally achiral luminescent materials could be tuned to chiral luminescent materials, as shown in Figure 1d. Because the chiral structure is part of the backbone, the chiral part is directly involved in the light-emitting process. Thus, a high performance with high g_{lum} is expected. We confirmed that these molecules have chiral optical properties in both density functional theory (DFT) calculations and experiments. We also expect that the idea of changing chirality through alkyl chains flipping may develop a new molecular model for advanced CP light emission materials.

2. Results and Discussion

Our strategy is achieved by the combination of alkyl chain and diketopyrrolopyrrole plane: an achiral alkyl chain is employed to connect the two nitrogen atoms in diketopy-rrolopyrrole (DPP) unit, and a closed-loop structure (CDPP) is formed, as demonstrated in Figure 2. Both the side chain and the conjugated backbone are achiral, the chiral center is formed after they are connected. The chiral centers are the two carbon atoms at the ends of the alkyl chain. Four groups/atoms being connected to the chiral center were sorted according to the Cahn–Ingold–Prelog priority rule [35]. One hydrogen atom (marked 3 in Figure 1d) forms a hydrogen bond with the oxygen atom in DPP, which has higher priority than the hydrogen atom marked 4. Therefore, the absolute configuration of these two chiral centers is discriminated. Additionally, the chirality of CDPP can be reversed by flipping the alkyl chain from one side of the DPP plane to the other side. It should be noted that to keep the molecule in a certain chirality, the alkyl chain should not be flipped. Once the alkyl chain is too long, it can be flipped at room temperature and the chirality of a molecule becomes uncertain. Therefore, overall achirality is anticipated.
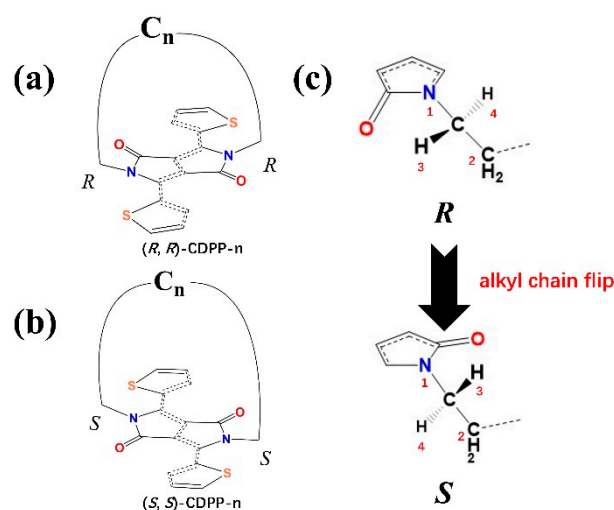

Figure 2. Molecular structure of (*R*, *R*)-CDPP (**a**); and (*S*, *S*)-CDPP (**b**); (**c**) The chiral center of (**a**,**b**), (**a**) can be changed into (**b**) through flipping the alkyl chain.

Molecules were labeled according to their chirality and the length of the alkyl chain, as shown in Figure 2. For example, the molecule with alkyl chain of 16 carbon atoms, under the R configuration, is labeled as (*R*, *R*)-CDPP-16. Molecular models were built by Gaussview6 and optimized at the B3LYP/6-31G* level by Gaussian09, and frequency analysis was performed to ensure that the fully optimized stationary point was found. Then, the electronic circular dichroism (ECD) and absorption of these molecules were calculated at the B3LYP/6-311++G* level.

2.1. Absorption Analysis

Figure 3a shows the calculated absorption spectra of these (*R*, *R*)-CDPP molecules. A series of absorption peaks are located at 200~400 nm and the highest absorption peak at around 530 nm. Through orbital analysis, it is found that the absorption at 530 nm originates from the transition of the highest occupied molecular orbitals (HOMO) to the lowest unoccupied molecular orbital (LUMO), whose contributions are both resulted from the electron delocalization of the whole DPP conjugated plane and part of the chiral center, as shown in Figure 3c. The absorption at 350 nm is attributed to the HOMO-2→LUMO transition. Figure 3d shows that the HOMO-2 is delocalized on both the DPP plane and the whole chiral center. These results indicate that the chiral center is indeed involved in the light absorption, especially the peak around 350 nm.
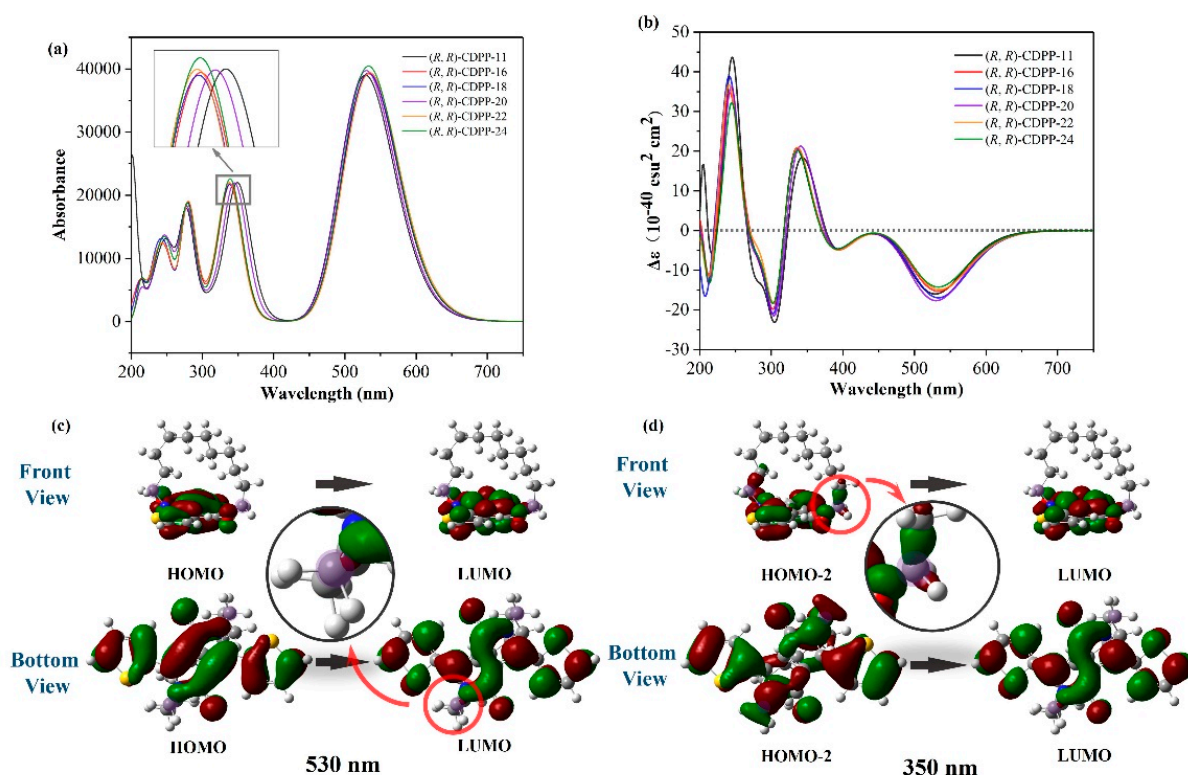
Figure 3. (**a**) calculated absorption spectra of (*R*, *R*)-CDPP molecules; (**b**) calculated ECD spectra of (*R*, *R*)-CDPP molecules; (**c**) the contour surfaces of frontier molecular orbitals (FMOs) involved in the absorption peak of (*R*, *R*)-CDPP-11 at 530 nm; and (**d**) the contour surfaces of FMOs involved in the absorption peak of (*R*, *R*)-CDPP-11 at 350 nm. The chiral centers are highlighted with light purple.

For further chiroptical properties, we calculated the rotatory strengths and ECD spectra of (*R*, *R*)-CDPPs. As shown in Figure 3b, the curves show two main positive peaks at 244 and 340 nm, and two negative peaks at 300 and 530 nm. The Cotton effect is also very obvious near 250 and 290 nm, which indicates good chiral optical properties [36,37].

The ECD curves of these (*S*, *S*)-CDPPs are basically the mirror images of (R, R)-CDPPs (Figure S1b). But it isn't for the (*S*, *S*)-CDPP-24. It shows a different pattern comparing to the

(*R*, *R*)-CDPP-24 curve. This is due to the overlong alkyl chain, in which the conformation lock fails. The conformation of the chiral center is not fixed for overlong chains. One chiral center of the built (*S*, *S*)-CDPP-24 becomes R state after relaxation as shown in Figure S10. This also suggests that to design a conformation lock chiral center the length of alkyl chain should not within a proper range.

2.2. Emission Analysis

The emission spectra of (*R*, *R*)-CDPP-(11, 16, 18, 20, 22, 24) were then calculated at B3LYP/6-311++G* level with time dependent DFT (TD-DFT), as shown in Figure 4a. CDPPs have two main luminescence regions, in which the three main emission peaks are 300, 340 and 608 nm. CDPPs show high luminous ability, and the intensity at 600 nm is relatively higher than that at 300 and 340 nm. The calculated Circularly Polarized Luminescence (CPL) spectra of (*R*, *R*)-CDPP-(11, 16, 18, 20, 22, 24) and (*S*, *S*)-CDPP-11 are also presented in Figure S8, which revealed circularly polarized emission ability in CDPP molecules.

$$g_{\text{lum}} = \frac{4|\boldsymbol{\mu}||\boldsymbol{m}|cos\theta}{|\boldsymbol{\mu}|^2 + |\boldsymbol{m}|^2} \tag{1}$$

The calculation of g_{lum} of (*R*, *R*)-CDPPs and (*S*, *S*)-CDPP-11 was then carried out according to equation 1, where $\boldsymbol{m}$ and $\boldsymbol{\mu}$ represent the magnetic and electric transition dipole moments, and θ stands for the angle between $\boldsymbol{m}$ and $\boldsymbol{\mu}$. The resulting data were then processed with Gaussian broadening and summarized in Figures 4b and S7 and Table 1.
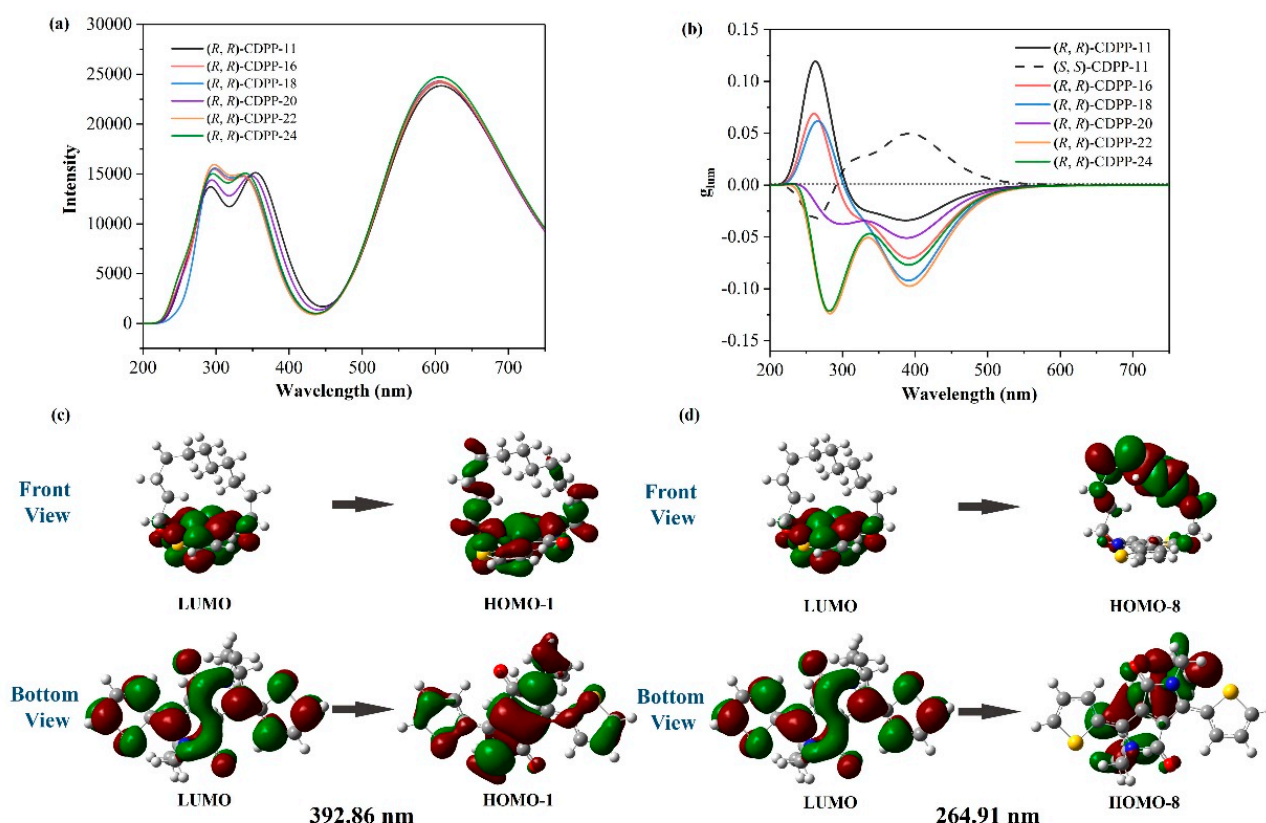
Figure 4. (**a**) calculated emission spectra of (*R*, *R*)-CDPP molecules; (**b**) calculated g_{lum} (after Gaussian broadening) of (*R*, *R*)-CDPP molecules and (*S*, *S*)-CDPP-11; (**c**) the contour surfaces of FMOs involved in the emission of (*R*, *R*)-CDPP-11, corresponding to the g_{lum} peak at around 392 nm; and (**d**) the contour surfaces of FMOs involved in the emission peak of (*R*, *R*)-CDPP-11, corresponding to the g_{lum} peak at 265 nm.

Table 1. The g_{lum} of (*R*, *R*)-CDPP.

g_{lum}	392 nm	608 nm
(*R*, *R*)-CDPP-11	-3.38×10^{-2}	-3.39×10^{-4}
(*S*, *S*)-CDPP-11	4.50×10^{-2}	3.78×10^{-4}
(*R*, *R*)-CDPP-16	-7.04×10^{-2}	-4.34×10^{-4}
(*R*, *R*)-CDPP-18	-9.20×10^{-2}	-5.06×10^{-4}
(*R*, *R*)-CDPP-20	-5.08×10^{-2}	-4.13×10^{-4}
(*R*, *R*)-CDPP-22	-9.73×10^{-2}	-5.06×10^{-4}
(*R*, *R*)-CDPP-24	-7.69×10^{-2}	-4.28×10^{-4}

As shown in Figure 4b, the curves of the calculated g_{lum} can be roughly divided into three sections. The first one ranges from 200 to 350 nm. In this section, the g_{lum} peaks (around 270 nm) of (*R*, *R*)-CDPPs change from positive high value (selectively emit left-handed circularly polarized light) to negative (selectively emit right-handed circularly polarized light), as the length of alkyl chain increases. Orbital composition analysis has been performed by the Hirshfeld method with Multiwfn 3.0 to explore the factors that influence these g_{lum} peaks [38]. The emission of the g_{lum} peaks of (*R*, *R*)-CDPPs at 200–350 nm involves multiple orbital transitions, as shown in Figures 4d and S4–S6. The DPP unit is divided into a chiral part and an achiral part, as illustrated in Figure S3. During the optical transition near 270 nm, the proportion of the orbital occupied on chiral parts (including the alkyl chain and the DPP chiral part) changes. For (*R*, *R*)-CDPP-11, 51.8% orbital is on chiral parts before transition. It becomes 99.4% after transition. Hence, the orbital chiral proportion increases by 47.6%. This increase gradually decreases and become −4.7% for (R, R)-CDPP-24, as shown in Table S2, indicating that the change in the g_{lum} peak of CDPP near 270 nm is influenced by the orbital occupancy on chiral parts. Detailed results are summarized in Tables S1 and S2. The second section ranges from 350 to 550 nm with peaks around 392 nm. As shown in Table 1, the $|g_{lum}|$ at 392 nm range from 3.38×10^{-2} to 9.73×10^{-2}, which are comparable to state-of-the-art small organic molecule CPL materials [39–41]. According to the Kasha's rule, this peak may not show as it is not the lowest excited level. However, the Kasha's rule may be overcome [42,43]. The last section ranges from 550 to 750 nm. Their $|g_{lum}|$ are between 3.39×10^{-4} to 5.06×10^{-4}, which are about two orders of magnitude smaller than that around 392 nm. The $|g_{lum}|$ at 608 nm is lower because the chiral proportion of orbitals are barely changed during the light-emitting process. For (*R*, *R*)-CDPP-11, the 392 nm peak mainly comes from LUMO→HOMO-8, as illustrated in Figure 4c. 51.2% of LUMO and 9.5% of HOMO-8 are on chiral parts, the chiral orbital change is 41.7%. The 608 nm peak attributes to LUMO→HOMO. The chiral proportions on orbitals alter from 51.2% to 61.8%. The chiral orbital change is only 10.6%. The details of orbital composition analysis are summarized in Table S1.

2.3. Chirality Transformation

In these molecules, the alkyl chain should maintain on a certain side of the DPP plane to keep the molecule in a certain chirality. We here investigated the chirality transformation when the alkyl chain flips. The relative energy and geometry changing from (*R*, *R*) state to (*S*, *S*) state were recorded. For CDPP-11, the alkyl chain is too short to flip. For others, at the beginning of flipping, total energies increased slowly with rotation as no significant deformation happened. When the alkyl chain approached the DPP conjugate plane and forces the plane to bend, total energies rapidly increased. The DPP plane recovered, and the molecular energy dropped to its lowest point after the alkyl chain successfully flipped to the other side. CDPP-16 has the highest energy barrier of 3.59 eV due to the shortest alkyl chain length. With increasing length, the energy barrier will decrease to 2.10, 1.23, 0.96 and 0.48 eV for CDPP-18, CDPP-20, CDPP-22 and CDPP-24, respectively. Details of the flipping process are shown in Figures 5 and S9.
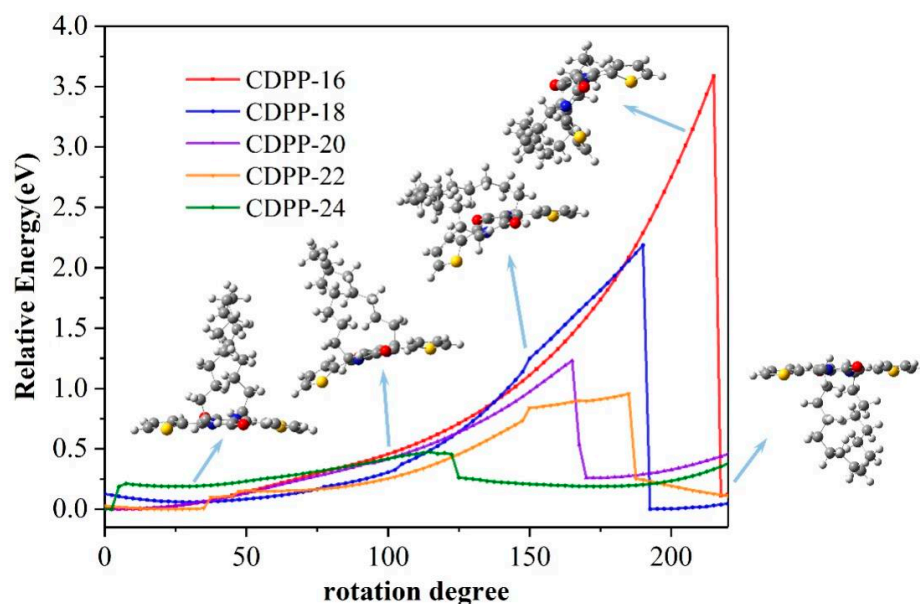
Figure 5. Geometries and relative energies during the flip of alkyl chains of (*R*, *R*)-CDPP-16, (*R*, *R*)-CDPP-18, (*R*, *R*)-CDPP-20, (*R*, *R*)-CDPP-22 and (*R*, *R*)-CDPP-24.

2.4. Calculation Verification

To verify our calculations, we further synthesized (*R*, *R*)-CDPP-11 and (*S*, *S*)-CDPP-11, and measured the CD and absorption spectra. The synthetic procedure is summarized in Supplementary Information. As shown in Figure 6, the CD spectra of (*R*, *R*)-CDPP-11 and (*S*, *S*)-CDPP-11 are symmetric in the experiment as well as DFT calculations. The CD peaks of (*R*, *R*)-CDPP-11 in the experiments located at 244, 279, 345 and 498 nm, match very well with the calculated peaks of 244, 305, 343 and 528 nm, respectively. Besides, the experimentally measured photoluminescence spectrum of CDPP-11, especially in the range of 500–750 nm (Figure S2) is also in good agreement with the TD–DFT calculation result. The consistency between both the experimental and calculated absorption, CD and emission spectra confirms the reliability of accurate prediction of the optical properties of these molecules.
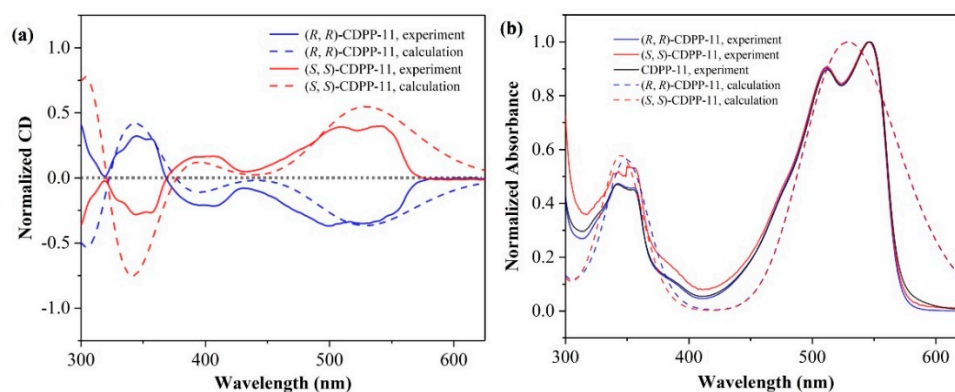
Figure 6. (**a**) Comparison between the experimental CD and calculated ECD spectra of CDPP-11; and (**b**) comparison between the experimental and calculated normalized absorption spectra of CDPP-11.

3. Conclusions

In this work, a new strategy to design CP light-emitting materials was proposed, by combining achiral side chains and achiral light-emitting groups. DFT calculated electronic circular dichroism, absorption spectra and emission spectra of these molecules indeed show chiroptical properties, with g_{lum} reaching -5.06×10^{-4}. By flipping alkyl chains, the

chiroptic of these molecules can be tuned, and a longer alkyl chain leads to a lower energy barrier during the flip. This strategy was further verified by experiments on a series of molecules. This combination makes it possible to change numerous achiral light-emitting materials to potentially high g_{lum} factor chiral luminescent materials by forming chiral center within the conjugation plane, allowing chiral center to participate in the emission progress. This work may provide a promising strategy for constructing high g_{lum} chiral light-emitting materials.

Supplementary Materials: The following supporting information can be downloaded at: https://www.mdpi.com/article/10.3390/photonics9080532/s1, Figure S1: (a) Calculated absorption spectrum of (*S*, *S*)-CDPP molecules, (b) Calculated ECD spectrum of (*S*, *S*)-CDPP molecules; Figure S2: Comparison between the experimental and calculated normalized emission spectrum of CDPP-11; Figure S3: The chiral and achiral fragments of the DPP plane; Figure S4: (a) Calculated g_{lum} (after Gaussian broadening) and emission spectrum of (*R*, *R*)-CDPP-16, (b) The contour surfaces of FMOs involved in the emission peak of (*R*, *R*)-CDPP-16 at 359.52 nm; Figure S5: (a) Calculated g_{lum} (after Gaussian broadening) and emission spectrum of (*R*, *R*)-CDPP-20, (b) The contour surfaces of FMOs involved in the emission peak of (*R*, *R*)-CDPP-20 at 279.62 nm; Figure S6: (a) Calculated g_{lum} (after Gaussian broadening) and emission spectrum of (*R*, *R*)-CDPP-24, (b) The contour surfaces of FMOs involved in the emission peak of (*R*, *R*)-CDPP-24 at 273.88 nm; Figure S7: (a) Calculated g_{lum} (after Gaussian broadening) and emission spectrum of (*R*, *R*)-CDPP-11, (b) Calculated g_{lum} (after Gaussian broadening) and emission spectrum of (*R*, *R*)-CDPP-16, (c) Calculated g_{lum} (after Gaussian broadening) and emission spectrum of (*R*, *R*)-CDPP-18, (d) Calculated g_{lum} (after Gaussian broadening) and emission spectrum of (*R*, *R*)-CDPP-20, (e) Calculated g_{lum} (after Gaussian broadening) and emission spectrum of (*R*, *R*)-CDPP-22, (f) Calculated g_{lum} (after Gaussian broadening) and emission spectrum of (*R*, *R*)-CDPP-24; Figure S8: Calculated CPL spectrum of (*R*, *R*)-CDPPs and (*S*, *S*)-CDPP-11; Figure S9: Geometry deforming of CDPP during the flip; Figure S10: The invalidated conformational lock of "(*S*, *S*)-CDPP-24"; Figure S11: The synthesis of DPP derivative; Figure S12: The synthesis of CDPP-11; Table S1: The orbital composition analysis of (*R*, *R*)-CDPP by Hirshfeld method in Multiwfn; Table S2: The proportion change of orbital composition during emission at around 270 nm. The chiral part includes the chiral fragment in DPP plane, and the alkyl chain.

Author Contributions: Conceptualization were done by L.W., H.L. and Y.L.; Theoretical calculation, software and original draft preparation were done by L.W. and T.H.; Y.Z., W.Y., G.L. and X.W. conceived and supervised the project; Reviewing and editing by L.W., T.H., W.O. and Y.Y. All authors have read and agreed to the published version of the manuscript.

Institutional Review Board Statement: Not applicable.

Informed Consent Statement: Not applicable.

Data Availability Statement: Not applicable.

Conflicts of Interest: The authors declare no conflict of interest.

References

1. Nakano, T.; Shikisai, Y.; Okamoto, Y. Helix-Sense-Selective Polymerization of 1-Phenyldibenzosuberyl Methacrylate by Free Radical Mechanism. *Proc. Jpn. Acad. Ser. B* **1995**, *71*, 251–255. [CrossRef]
2. Brandt, J.R.; Salerno, F.; Fuchter, M.J. The Added Value of Small-molecule Chirality in Technological Applications. *Nat. Rev. Chem.* **2017**, *1*, 0045. [CrossRef]
3. Nolte, R.J.M. Helical Poly(isocyanides). *Chem. Soc. Rev.* **1994**, *23*, 11–19. [CrossRef]

4.   Kane-Maguire, L.A.P.; Wallace, G.G. Chiral Conducting Polymers. *Chem. Soc. Rev.* **2010**, *39*, 2545–2576. [CrossRef] [PubMed]
5.   Jin, X.; Sang, Y.; Shi, Y.; Li, Y.; Zhu, X.; Duan, P.; Liu, M. Optically Active Upconverting Nanoparticles with Induced Circularly Polarized Luminescence and Enantioselectively Triggered Photopolymerization. *ACS Nano* **2019**, *13*, 2804–2811. [CrossRef] [PubMed]
6.   Kumar, J.; Thomas, K.G.; Liz-Marzan, L.M. Nanoscale Chirality in Metal and Semiconductor Nanoparticles. *Chem. Commun.* **2016**, *52*, 12555–12569. [CrossRef] [PubMed]
7.   Bisht, K.K.; Parmar, B.; Rachuri, Y.; Kathalikattil, A.C.; Suresh, E. Progress in the Synthetic and Functional Aspects of Chiral Metal–organic Frameworks. *CrystEngComm* **2015**, *17*, 5341–5356. [CrossRef]
8.   Brandt, J.R.; Wang, X.; Yang, Y.; Campbell, A.J.; Fuchter, M.J. Circularly Polarized Phosphorescent Electroluminescence with a High Dissymmetry Factor from PHOLEDs Based on a Platinahelicene. *J. Am. Chem. Soc.* **2016**, *138*, 9743–9746. [CrossRef]
9.   Yang, Y.; da Costa, R.C.; Smilgies, D.M.; Campbell, A.J.; Fuchter, M.J. Induction of Circularly Polarized Electroluminescence from an Achiral Light-Emitting Polymer via a Chiral Small-Molecule Dopant. *Adv. Mater.* **2013**, *25*, 2624–2628. [CrossRef]
10. Xiang, D.; Wang, X.; Jia, C.; Lee, T.; Guo, X. Molecular-Scale Electronics: From Concept to Function. *Chem. Rev.* **2016**, *116*, 4318–4440. [CrossRef]
11. Mao, X.; Zhao, H.; Luo, L.; Tian, D.; Li, H. Highly Sensitive Chiral Recognition of Amino Propanol in Serum with R-mandelic Acid-linked Calix[4]arene Modified Graphene. *J. Mater. Chem. C* **2015**, *3*, 1325–1329. [CrossRef]
12. Guo, L.; Huang, Y.; Zhang, Q.; Chen, C.; Guo, D.; Chen, Y.; Fu, Y. Electrochemical Sensing for Naproxen Enantiomers Using Biofunctionalized Reduced Graphene Oxide Nanosheets. *J. Electrochem. Soc.* **2014**, *161*, B70–B74. [CrossRef]
13. Zhang, Q.; Huang, Y.; Guo, L.; Chen, C.; Guo, D.; Chen, Y.; Fu, Y. DNA-based Nanocomposite as Electrochemical Chiral Sensing Platform for the Enantioselective Interaction with Quinine and Quinidine. *New J. Chem.* **2014**, *38*, 4600–4606. [CrossRef]
14. Zhang, D.W.; Li, M.; Chen, C.F. Recent Advances in Circularly Polarized Electroluminescence Based on Organic Light-emitting Diodes. *Chem. Soc. Rev.* **2020**, *49*, 1331–1343. [CrossRef] [PubMed]
15. Wagenknecht, C.; Li, C.M.; Reingruber, A.; Bao, X.H.; Goebel, A.; Chen, Y.A.; Zhang, Q.; Chen, K.; Pan, J.W. Experimental Demonstration of a Heralded Entanglement Source. *Nat. Photonics* **2010**, *4*, 549–552. [CrossRef]
16. Willner, A.E.; Huang, H.; Yan, Y.; Ren, Y.; Ahmed, N.; Xie, G.; Bao, C.; Li, L.; Cao, Y.; Zhao, Z.; et al. Optical Communications Using Orbital Angular Momentum Beams. *Adv. Opt. Photonics* **2015**, *7*, 66–106. [CrossRef]
17. Shen, C.; Loas, G.h.; Srebro-Hooper, M.; Vanthuyne, N.; Toupet, L.; Cador, O.; Paul, F.; López Navarrete, J.T.; Ramírez, F.J.; Nieto-Ortega, B.; et al. Iron Alkynyl Helicenes: Redox-Triggered Chiroptical Tuning in the IR and Near-IR Spectral Regions and Suitable for Telecommunications Applications. *Angew. Chem. Int. Ed.* **2016**, *55*, 8062–8066. [CrossRef]
18. Kim, D.Y. Potential Application of Spintronic Light-emitting Diode to Binocular Vision for Three-dimensional Display Technology. *J. Korean Phys. Soc.* **2006**, *49*, S505–S508.
19. Long, G.; Adamo, G.; Tian, J.; Klein, M.; Krishnamoorthy, H.N.S.; Feltri, E.; Wang, H.; Soci, C. Perovskite Metasurfaces with Large Superstructural Chirality. *Nat. Commun.* **2022**, *13*, 1551. [CrossRef]
20. Sroor, H.; Huang, Y.W.; Sephton, B.; Naidoo, D.; Vallés, A.; Ginis, V.; Qiu, C.W.; Ambrosio, A.; Capasso, F.; Forbes, A. High-purity Orbital Angular Momentum States from a Visible Metasurface Laser. *Nat. Photonics* **2020**, *14*, 498–503. [CrossRef]
21. Cai, X.; Wang, J.; Strain Michael, J.; Johnson-Morris, B.; Zhu, J.; Sorel, M.; O'Brien Jeremy, L.; Thompson Mark, G.; Yu, S. Integrated Compact Optical Vortex Beam Emitters. *Science* **2012**, *338*, 363–366. [CrossRef] [PubMed]
22. Xiao, L.; An, T.; Wang, L.; Xu, X.; Sun, H. Novel Properties and Applications of Chiral Inorganic Nanostructures. *Nano Today* **2020**, *30*, 100824. [CrossRef]
23. Döring, A.; Ushakova, E.; Rogach, A.L. Chiral Carbon Dots: Synthesis, Optical Properties, and Emerging Applications. *Light Sci. Appl.* **2022**, *11*, 75. [CrossRef] [PubMed]
24. Long, G.; Jiang, C.; Sabatini, R.; Yang, Z.; Wei, M.; Quan, L.N.; Liang, Q.; Rasmita, A.; Askerka, M.; Walters, G.; et al. Spin Control in Reduced-dimensional Chiral Perovskites. *Nat. Photonics* **2018**, *12*, 528–533. [CrossRef]
25. Long, G.; Zhou, Y.; Zhang, M.; Sabatini, R.; Rasmita, A.; Huang, L.; Lakhwani, G.; Gao, W. Theoretical Prediction of Chiral 3D Hybrid Organic–Inorganic Perovskites. *Adv. Mater.* **2019**, *31*, 1807628. [CrossRef] [PubMed]
26. Kulkarni, C.; van Son, M.H.C.; Di Nuzzo, D.; Meskers, S.C.J.; Palmans, A.R.A.; Meijer, E.W. Molecular Design Principles for Achieving Strong Chiroptical Properties of Fluorene Copolymers in Thin Films. *Chem. Mater.* **2019**, *31*, 6633–6641. [CrossRef]
27. Di Nuzzo, D.; Kulkarni, C.; Zhao, B.; Smolinsky, E.; Tassinari, F.; Meskers, S.C.J.; Naaman, R.; Meijer, E.W.; Friend, R.H. High Circular Polarization of Electroluminescence Achieved via Self-Assembly of a Light-Emitting Chiral Conjugated Polymer into Multidomain Cholesteric Films. *ACS Nano* **2017**, *11*, 12713–12722. [CrossRef]
28. Wan, L.; Wade, J.; Salerno, F.; Arteaga, O.; Laidlaw, B.; Wang, X.; Penfold, T.; Fuchter, M.J.; Campbell, A.J. Inverting the Handedness of Circularly Polarized Luminescence from Light-Emitting Polymers Using Film Thickness. *ACS Nano* **2019**, *13*, 8099–8105. [CrossRef]
29. Li, T.; Guo, H.; Wang, Y.; Ouyang, G.; Wang, Q.Q.; Liu, M. Chiral Macrocycle-induced Circularly Polarized Luminescence of a Twisted Intramolecular Charge Transfer Dye. *Chem. Commun.* **2021**, *57*, 13554–13557. [CrossRef]
30. Jimenez, J.; Cerdan, L.; Moreno, F.; Maroto, B.L.; Garcia-Moreno, I.; Lunkley, J.L.; Muller, G.; de la Moya, S. Chiral Organic Dyes Endowed with Circularly Polarized Laser Emission. *J. Phys. Chem. C* **2017**, *121*, 5287–5292. [CrossRef]
31. Barnett, C.J.; Drake, A.F.; Mason, S.F. The Polarized Luminescence and Vibrational Optical Activity of Calycanthine. *Bull. Soc. Chim. Belg.* **1979**, *88*, 853–862. [CrossRef]

32. Leventis, A.; Royakkers, J.; Rapidis, A.G.; Goodeal, N.; Corpinot, M.K.; Frost, J.M.; Bucar, D.K.; Blunt, M.O.; Cacialli, F.; Bronstein, H. Highly Luminescent Encapsulated Narrow Bandgap Polymers Based on Diketopyrrolopyrrole. *J. Am. Chem. Soc.* **2018**, *140*, 1622–1626. [CrossRef] [PubMed]

33. Hahn, R.; Bohle, F.; Fang, W.; Walther, A.; Grimme, S.; Esser, B. Raising the Bar in Aromatic Donor-Acceptor Interactions with Cyclic Trinuclear Gold(I) Complexes as Strong Pi-donors. *J. Am. Chem. Soc.* **2018**, *140*, 17932–17944. [CrossRef]

34. Zhao, Y.; Sakai, N.; Matile, S. Enolate Chemistry with Anion-pi Interactions. *Nat. Commun.* **2014**, *5*, 3911. [CrossRef] [PubMed]

35. Moss, G.P. Basic Terminology of Stereochemistry (IUPAC Recommendations 1996). *Pure Appl. Chem.* **1996**, *68*, 2193–2222. [CrossRef]

36. De Cremer, L.; Verbiest, T.; Koeckelberghs, G. Influence of the Substituent on the Chiroptical Properties of Poly(thieno[3,2-b]thiophene)s. *Macromolecules* **2008**, *41*, 568–578. [CrossRef]

37. Blout, E.R.; Stryer, L. Anomalous Optical Rotatory Dispersion of Dye: Polypeptide Complexes. *Proc. Natl. Acad. Sci. USA* **1959**, *45*, 1591–1593. [CrossRef]

38. Lu, T.; Chen, F. Multiwfn: A Multifunctional Wavefunction Analyzer. *J. Comput. Chem.* **2012**, *33*, 580–592. [CrossRef]

39. Zhang, X.; Zhang, Y.; Li, Y.; Quan, Y.; Cheng, Y.; Li, Y. High Brightness Circularly Polarized Blue Emission from Non-doped OLEDs Based on Chiral Binaphthyl-pyrene Emitters. *Chem. Commun.* **2019**, *55*, 9845–9848. [CrossRef]

40. Zhang, X.; Zhang, Y.; Zhang, H.; Quan, Y.; Li, Y.; Cheng, Y.; Ye, S. High Brightness Circularly Polarized Organic Light-Emitting Diodes Based on Nondoped Aggregation-Induced Emission (AIE)-Active Chiral Binaphthyl Emitters. *Org. Lett.* **2019**, *21*, 439–443. [CrossRef]

41. Sakai, H.; Shinto, S.; Kumar, J.; Araki, Y.; Sakanoue, T.; Takenobu, T.; Wada, T.; Kawai, T.; Hasobe, T. Highly Fluorescent [7] Carbohelicene Fused by Asymmetric 1,2-dialkyl-substituted Quinoxaline for Circularly Polarized Luminescence and Electroluminescence. *J. Phys. Chem. C* **2015**, *119*, 13937–13947. [CrossRef]

42. Wang, H.; Wang, J.; Zhang, T.; Xie, Z.; Zhang, X.; Sun, H.; Xiao, Y.; Yu, T.; Huang, W. Breaching Kasha's Rule for Dual Emission: Mechanisms, Materials and Applications. *J. Mater. Chem. C* **2021**, *9*, 10154–10172. [CrossRef]

43. Shi, L.; Yan, C.; Guo, Z.; Chi, W.; Wei, J.; Liu, W.; Liu, X.; Tian, H.; Zhu, W.H. De Novo Strategy with Engineering Anti-Kasha/Kasha Fluorophores Enables Reliable Ratiometric Quantification of Biomolecules. *Nat. Commun.* **2020**, *11*, 793. [CrossRef] [PubMed]